Optical Mapping of Tip-Enhanced Raman Spectroscopy (TERS)

Thesis submitted in partial fulfilment of the requirements for the degree of Bachelor of Science in Electronic and Communication Engineering

By

Md. Nasimuzzaman Mishuk

Department of Electrical and Electronic Engineering

BRAC University

Declaration

I, hereby, declare that the thesis “Optical Mapping of Tip-Enhanced Raman Spectroscopy (TERS)” is based on self-derived results. Materials that support my work by other researchers are mentioned in the reference section. This thesis, neither in whole nor in part, has been previously submitted for any degree

_____

Candidate

Md. Nasimuzzaman Mishuk

ID: 13110041

Certified by:

_____

Dr. Md. Mosaddequr Rahman

Supervisor

Lecturer

Department of EEE

BRAC University, Dhaka

_____

Md. Anamul Hoque

Co-Supervisor

Lecturer

Department of EEE

BRAC University, Dhaka

Acknowledgement

First of all, I would like to thank my supervisor Dr. Md. Mosaddequr Rahman sir for allowing me to pursue my thesis in my desired field. I consider myself lucky that he agreed to be the supervisor of my thesis. Then, I would like to express my sincere gratitude to my co-supervisor Md. Anamul Hoque sir for his patience, motivation, and immense knowledge. His guidance helped me in all the time of research and writing of this thesis study.

Abstract

Imaging technique with high-sensitivity and high-spatial-resolution at single molecular level is always a desired aspect to the researchers. In association with scanning probe microscopy and surface-enhanced Raman spectroscopy (SERS), a new technology has shown the light of hope to achieve what was thought as unachievable earlier, named tip-enhanced Raman spectroscopy (TERS). An essential tip is used in TERS instead of rough metal film. This tip gives the information of the topology of the target molecule by scanning probe technique and can magnify the Raman signal largely without any special sample preparation. Between this metal tip and surface, a 'hot-spot' is formed when the laser beam is applied. Conventionally in TERS theory, Raman signal enhancement factor is approximately equal to the fourth power of the local field enhancement factor at the 'hot-spot'. In this thesis, the localized electric field in the vicinity of the metallic tip of TERS was examined and the effect of different polarization of source in mapping TERS was observed with Finite-Difference Time-Domain method (FDTD) simulation. For this simulation, tip radius and distance between tip and substrate were kept constant and incident wavelengths were varied. For the sake of simulation, Lumerical simulation software was used because of its high accuracy.

Keywords: Tip-enhanced Raman Spectroscopy, Localized surface plasmon resonance, Spatial resolution, enhancement factor, Finite-Difference-Time-Domain.

Table of Contents

List of Figures

List of Tables

This page was intentionally left blank

1. Preamble

Raman scattering is an inelastic scattering of light. In 1928, Raman spectroscopy was introduced by Sir Chandrasekhara Venkata Raman an Indian Physicist, together with K. S. Krishnan. For this tremendous contribution in Physics, Sir C. V. Raman got Nobel prize in 1930.

Raman spectroscopy is a label-free technique (1) which means no additional molecule is needed to detect the targeted one. As a result, Raman spectroscopy has a tremendous prospect in the field characterization of materials. This systematic technique can be used to exposes knowledge about the formation (3), electronic structure (4), permeability (5), structural and optical properties (6) and also chemical bonding (7) of material through the observation of molecular vibrations. The application of Raman Spectroscopy has a wide variety. Starting from food and beverage to energy, geology, and environment to in situ analysis, polymers and materials to nano-materials, semiconductors, and optoelectronics to art and museum (2). Having all those potentials in the characterization of materials the scattered Raman signal needs to undergo a few improvements to maximize our desired outcome. It is because inherently Raman scattering is very weak. Various techniques are existing in the field to improve the Raman signal. Surface-enhanced Raman spectroscopy (SERS) was introduced to improve the signal strength. SERS is one type spectroscopy in which all the examining molecules need to be on the surface. The enhancement comes from the Plasmon resonance of that surface. More particularly, the improvement of Raman scattering happens by the molecules adsorbed on the metal substrates (surface) (8). By SERS, multiple orders of magnitudes of Raman signal can be improved that is why it is mainly used. SERS has a problem with its universality. For instance, the substrate is needed to be remodeled and prepared again from scratch every time while performing SERS for a particular molecule. The whole process is time-consuming and cost ineffective. The primary reason behind changing the substrate every time is, the ultimate result differs from sample to sample and the preparation of substrate has a significant impact on the outcome (1). Moreover, it is not fruitful for a single molecule as it is difficult to detect the real signal by this technique in real space (9, 12-14). Along with that, the samples prepared in SERS are likely to tarnish in the air quickly which is a drawback again and results in an ambiguous result from our targeted molecule which means Raman signal that is extracted can’t be distinguished whether it has come from the intrinsic sample or the contaminated one (9-11).

Keeping all the above things in consideration, TERS was introduced to conquer the flaws which

were affecting a conclusive result in SERS.

TERS is the unification of surface enhanced Raman spectroscopy (SERS) and scanning probe microscopy (SPM). This mechanism enables the chemical imaging of surfaces at the nanometer length scale. In this technique, scanning probe microscope needs to have a high spatial resolution to characterize Raman spectroscopy (15). TERS cancels out most of the flaws and introduces an approach for computable SERS imaging with nanometer resolution. An essential tip is used in TERS instead of rough metal film. This tip gives the information of the topology of the target molecule by scanning probe technique. This tip can magnify the Raman signal mainly without any special sample preparation (16).

1.2 Scope Of the Thesis

In this thesis, the localized electric field in the vicinity of the metallic tip of TERS will be examined, and the conventional TERS theory will be verified with Finite-Difference Time-Domain (FDTD) simulation. While doing so, graphene surface and tip will also be used along with silver and gold. The justification behind using graphene is, it is highly promising material. It has a very high electrical conductivity which may induce a very high enhancement.

The specific objectives of this thesis are structured as follows:

In chapter 2, basics from Raman scattering was delineated first. Then, the evolution of enhancement techniques like SERS and TERS were described. Along with that, the underlying mechanisms of enhancement was defined.

Chapter 3 belongs to the methodology. In this section, the justification and principles of the Finite-Domain-Time-Difference method were described. Besides that, a brief idea about the simulation software, Lumerical was given.

Results and discussions are covered in chapter 4. Here, the output of the simulations was described with figures. A Proper explanation of the results was discussed in this area.

Finally, the thesis was wrapped up in the concluding sector referring some possible improvements of TERS.

2. Literature Review

2.1 Raman Scattering

2.1.1 Theory

From the previous chapter, we know that Raman scattering is inelastic. The meaning of inelastic scattering is observable from the figure below. When an electron is excited by photons of applied light, it jumps from ground state to higher sates. While scattering, there are various possible things might happen. To explain Raman scattering, I have mentioned three of them here. From the figure delineated below, we can see an elastic scattering of light namely, Rayleigh scattering. This scattering is responsible for visible lights and falls under visible spectroscopy. After that, there are two inelastic scattering. They are Stokes Raman scattering and Anti-Stokes Raman scattering. When a scattered photon has an energy lower than the applied

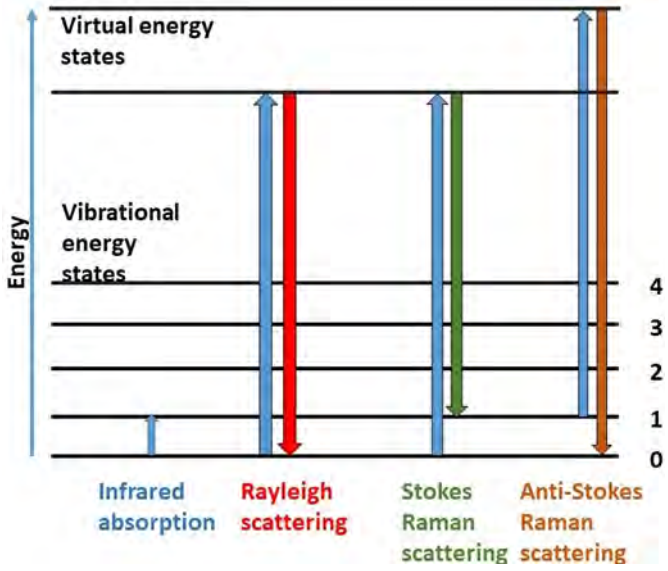

Figure 1: Energy Band diagram showing the spectroscopic transitions involved with Rayleigh, and Raman scattering

photon(light) by some quantum and electron comes back to the first vibrational state, Stokes Raman scattering occurs which is also called positive Raman shift. On the other hand, when a scattered photon has higher energy than the incident photon and it assigns the molecule at the ground state is called Anti-Stokes Raman scattering or negative Raman shift as an alternative.

Raman scattering of a molecule is identical to the fingerprint of a human being. As we know, the fingerprint is the most useful tool for distinguishingpeople from one another. Like that, the organization of Raman spectrum is an intrinsic characteristic of a particular molecule which means two different particles cannot have the same Raman spectrum (17). Raman can access the chemical content of a molecule system through the observation of molecular vibrations (18). Along with that, the whole process is label-free which means we do not need any alien molecules to run the operation. Consequently, Raman exposes a considerable amount of possibilities in front of us.

2.1.2 Applications of Raman spectroscopy

As we know Raman scattering can characterize a sample without labeling and destructing, it has a wide variety of use in the field of biological materials, medicine, environment, nano-materials, in arts and museums (2), Cell imaging (20,22), Tissue imaging (21-22), cancerdiagnosis.

Talking about biological materials, using Raman spectroscopy we can easily excerpt biological information as it can measure the chemical structure of a molecule. “Fresh plant tissue, formalin-fixed and fresh frozen mammalian tissue, fixed cells and biofluids” (22), etc. can be mapped by Raman spectroscopy and later, those data are used to characterize.

Pigments are essential for coloring our clothes and paintings, varnishing our furniture, etc. The present scientific way of detecting dye has problems. The sample amount has to very small, and eventually, it gets destructed. On the other hand, as we know Raman Spectroscopy is no destructive and label-free which make it the perfect technique for examining the pigment of color with ease. Correspondingly, identification of pigment, date analysis or recognition of artifice can be efficiently obtained by Raman Scattering. For instance, Raman spectroscopy was applied in a wall painting of a profane figure found from Skopje fortress in Macedonia.

Figure 2: Foundation of Skopje Fortress (left) and a paint of profane figure that was later examined under micro-Raman spectroscopy(right)

The result found after applying the micro-Raman was fascinating. It provided the information about the usage of organic and inorganic pigments which eventually proved that the Skopje Fortress was reconstructed in the 19th century [23].

Usage in *vitro* fertilization (IVF) is another fascinating application of Raman scattering. Alistair Elfick et al. have developed a non-destructive mechanism in quest of examining the features of sperm to be used in fertility treatments at the University of Edinburgh. To evaluate the quality of DNA, they applied Raman spectroscopy to investigate single sperm cells. After that, the healthiest sperm can be used in an intracytoplasmic sperm injection. In this injection, a single sperm is nominated and inoculated into the egg (24-25). The Alistair Elfick et al. team is hopeful about theincrease of the chances of conception for the couples using *in vitro*fertilization (IVF) to have children because of this method.

So, the above discussion is a clear indication that Raman spectroscopy has a lot to give us in the field of material science, medicine, etc. through its outstanding characteristics.

2.1.3 Limitations

Along with all those potentials above, Raman scattering has some shortcomings too. That is, Raman scattering is genuinely low. It is because, while measuring Raman scattering Stokes

scattering is used which has a higher intensity than Anti-stokes scattering (19) but Stokes scattering occurs at a lower energy than Rayleigh scattering. As a result, intrinsically Raman scattering is very weak ($10^{-7}$of total scattered light approximately). According to the Boltzmann distribution, excited vibrational energy levels are less populated than the ground state. Hence, anti-Stokes is less intense because the scattering occurs from the less populated state. We can make the issue even more evident in the equations below:

$$I_{tot,x}(Stokes) = \frac{h.N.(\overline{\nu_0} - \overline{\nu_v})^4}{8.{\varepsilon_0}^2.c.\overline{\nu_v}} \frac{45.\ \alpha'^2 + 13.\gamma'^2}{45} \frac{E^2}{1 - e^{-h.c.\frac{\overline{\nu_v}}{kT}}} \quad \text{.....1 [19]}$$

$$I_{tot,x}(Anti - stokes) = \frac{h.N.(\overline{\nu_0} + \overline{\nu_v})^4}{8.{\varepsilon_0}^2.c.\overline{\nu_v}} \frac{90.\ \alpha^2 + 14.\gamma^2}{45} \frac{E^2}{e^{h.c.\frac{\overline{\nu_v}}{kT}} - 1} \quad \text{.....2 [19]}$$

If we observe their denominator, it is apparent that the denominator of equation one will always be smaller than the denominator of equation 2. As a consequence, the total incidence of Stokes scattering is greater than Anti-Stokes scattering. On the other hand, stokes scattering occurs at lower energy than Rayleigh. As we use Stokes scattering while measuring Raman scattering, it inherently becomesfragile for the above reason (19).

2.2 Basic Principles behind the enhancements

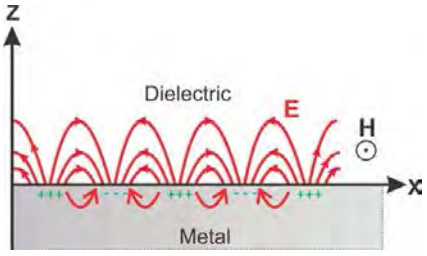

Figure 3: Interaction between metallic surface and dielectric and the creation of surface plasmons (34)

2.2.1 Surface Plasmon

The intercommunication between electromagnetic waves and metallic tips increases the oscillation of outer shell electrons of metallic tips. The increased oscillation has a phase

difference with the incident electric field (31, 32). This new oscillation shifts the free electron in comparison with the position of positively charged unit cell of the atom. At a particular frequency, these free electrons can escape the surface and the whole volume's charge density. At this stage, they are called plasmons. At the gap between a metallic surface and dielectrics, plasmon becomes surface plasmon (31,33). Alternatively, at the surface of the metallic structure the total oscillations of the electron density are also called surface plasmons (31).

If an electromagnetic wave is applied in the surface plasmons, their oscillations increase significantly. This increased oscillation can increase the electric field at the vicinity of two metallic surface and dielectric material.

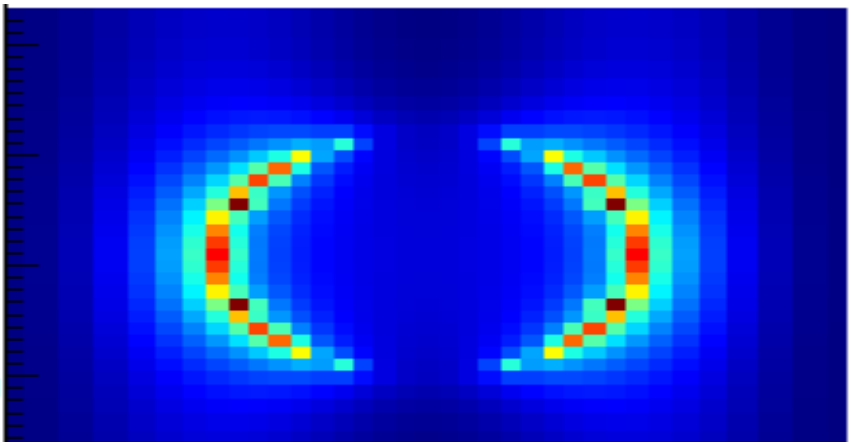

Figure 4: Localized surface plasmon observed on nanoholes place on a thin gold film

2.2.2 Localized surface plasmons

Localized surface plasmons are special kind of surface plasmons. Surface plasmons become confined when metallic nanostructures are smaller in proportion to the wavelength of the applied electromagnetic wave (34).

2.3 Fundamentals of SERS its limitations

2.3.1 Theory

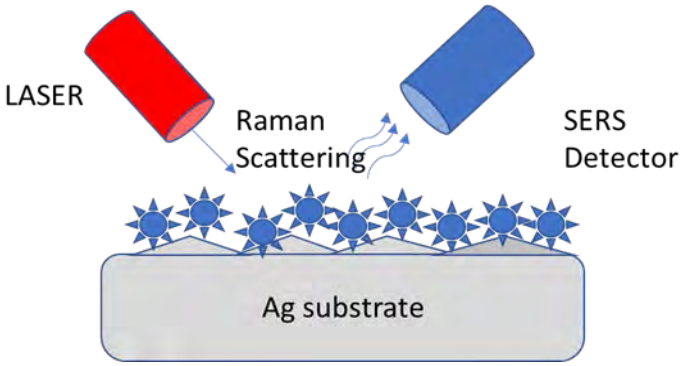

Figure 5: Schematics diagram of Surface enhanced Raman spectroscopy

From the discussion of the Raman scattering, it is evident to us that Raman spectroscopy single-handedly can solve numerous problems and open up a lot of unknowns in front of us. At the same time, from Boltzmann distribution along with the equation 1 and 2, we are well aware of the limitations of intrinsic Raman spectroscopy. Due to the above reasons, the applicability of Raman scattering was restricted for many years. As a consequence, to use Raman scattering more efficiently enhancement techniques appeared in the course of time. In the 1970s, a breakthrough happened in the field of Raman spectroscopy. The first enhancement mechanism was inventedat that occasion. Chemistry World, a monthly chemistry news magazine published by the Royal Society of Chemistry published an article in 2015 named as "**SERS and the rise of the Raman empire**."It said, "We should remember that the discovery of surface-enhanced Raman spectroscopy (SERS) was a historic breakthrough which has been helping save lives in the field of healthcare and finding use in applications such as medical diagnostics, food safety, national security, environmental monitoring, fine art preservation, financial security and rapid screening.It deserves more recognition" (35).

Through SERS an enhancement factor of $10^6 - 10^{12}$is obtainable. The mechanism of SERS has remained abstruse from the very beginning of its discovery. The total enhancement mechanism is described as a product of two different mechanisms. It is becauseRaman scattering is directly proportional to the induced dipole moment. On the other hand, the induced dipole moment is the product of Raman polarizability and the magnitude of the incident electromagnetic field. As a consequence, we need both chemical and electromagnetic enhancement mechanism to describe SERS concisely (36). The contribution of chemical enhancement mechanism is about a factor of 100. In this mechanism, a charge-transfer state is formulated in the vicinity of the metal surface and adsorbate molecules (38,39). The charge-transfer state electrons become excited and move from a lower energy level to a higher energy level(37). Charge-transfer state increases the path of resonant excitation which eventually increase the probability of Raman transition. Chemical enhancement mechanism is highly dependent on surface and the molecule that is used while experimenting. A specific molecule must be directly adsorbed on a particular roughened surface to obtain chemical enhancement.

Electromagnetic enhancement mechanism is responsible for the enhancement of the magnitude of the SERS originating from the local field and the scattered field. Electromagnetic mechanism depends on the LSPR described in the previous chapter. A hot spot is created at the node of surface-sample molecule by LSPR which can generate enhancement factor from $10^5 - 10^{10}$ (34).

Enhancement factor is the ratio of normalized SERS signal and normal Raman signal. It is used as the increasing indicator of enhancement. Theoritically, it is said the enhancement factor is E^4(36). Mathematically, it looks like the following,

$$EF_{SERS} = \frac{I_{SERS}/N_{SERS}}{I_{NRS}/N_{NRS}} \quad \text{..... (3) (34)}$$

Where, N_{NRS} andN_{SERS} are the number of molecules participating in normal Raman spectroscopy and SERS signals. Whereas, I_{NRS} and I_{SERS} represent the intensities of SERS and normal Raman

spectroscopy signals.

2.3.2 Applications

As we know that SERS can produce enhancement factor from $10^5 - 10^{10}$, it has impact on various fields. Some of them are briefly discussed in this section.

Biosensors

As SERS is highly sensitive technique, it is used as to produce biosensors. This sensor can collect data and later can identify them very efficiently. It can collect data of the diseases like Cancer, Alzheimer, Parkinson's etc. in an efficient way (40).

Arts and archeology

SERS plays an important role in preserving the ancient art and archeological things like,

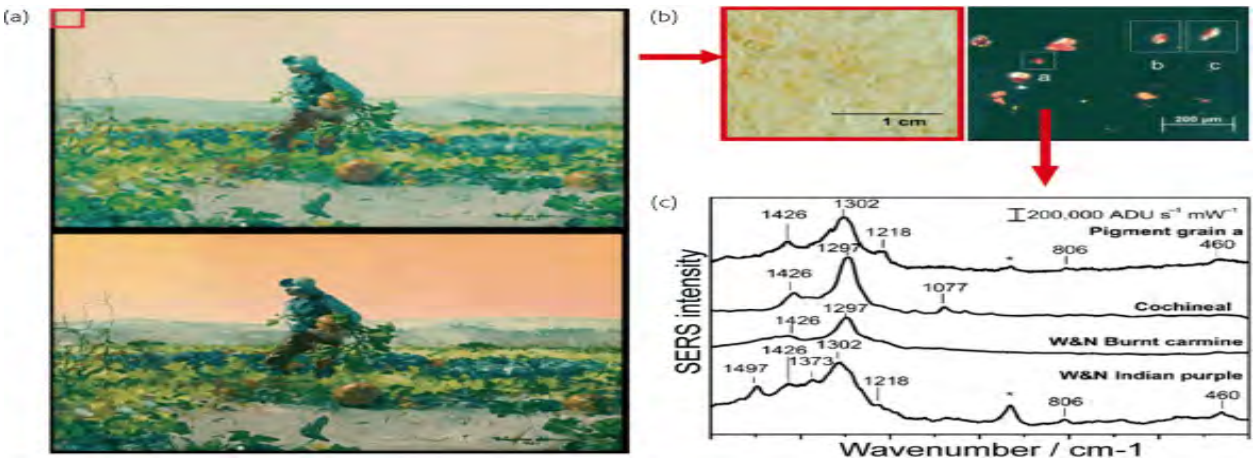

Figure 6: An watercolor painting by Winslow homer named 'For to be a farmer's boy'. (a) (upper part) painting as it seen now-a-days and (b) how it is developed by SERS analysis. In (b) and (c) the analysis of pigments are shown. It was taken from Elsevier with permission. License number: 4252890682286 (40)

paintings.

It is to essential to bear in mind that, in old paintings the concentration of chemicals is very low

and also has a small amount quantity. So, we have to have a technique that can identify the pigments from that little amount. SERS is capable of doing that. It can easily identify natural pigments and glazes (40). As a consequence, SERS has become a popular tool in this field.

2.3.3 Limitations

Overcoming the diffraction limit of light and achieving subnanometer resolution with SERS is very challenging. As a consequence, SERS cannot provide subnanometre resolution.

Another major limitation of SERS is, it is not possible to detect the correspondingconformation of molecular vibrational state, but it is immensely valuable. For instance, to understand the molecule, to produce Nanomachine, to improve the performance of biological molecules, to produce molecular memory or logic devices, etc., the analysis of vibrational states works as an essential tool.

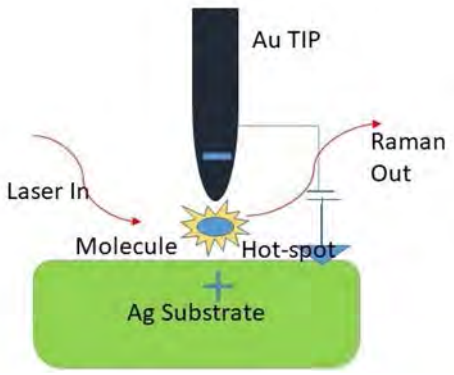

Figure 7: Schematic diagram of Tip – enhanced Raman spectroscopy

2.4 Fundamentals of TERS and its advantages

2.4.1 Theory

The notable mechanisms which play a pivotal role - the EM and CHEM mechanisms - in the augmentation of TERS experiments. The global TERS community have made great strides in their understanding of the quantum mechanical phenomenon of the enhancements in TERS, which has the potential of paving the way for elevated lateral resolution. The factor that causes the augmentation field that is engaged in EM for TERS is the sharp tip, which differs from that of SERS, metal surface in that case. The structure of the tip paves way for a significantly elevated number of surface charges at its summit, causing highly spatially localized electromagnetic fields. The field intensity sees a further increase as it advances towards the tip at a closeness range of (1-2 nm) to a plasmonic substrate. In the space between the tip and the substrate, the tip and surface plasmons collectively generates a spatially confined field. This phenomenon is popularly called the gap-mode effect. In between the narrow space in the tipsubstrate system, the augmentation which occurs there obeys a d^ (-10) dependence, where d represents the distance which is in between the tip and the substrate.

The tip material and the structure along with the incident laser polarization, focus, relative angle and wavelength, among other factors, are responsible for governing the nature of the restricted field. The various recent theoretical studies, which have made attempts to investigate EM for diverse tip-substrate structure and material incorporation in the hunt for an optimal apparatus, have applied finite-difference time-domain (FDTD) modeling and analytical theory. The tip has

been illustrated as an idealized smooth surface in all cases. The structure at the bottom of the tip which is an approximation of roughly the last 100 nm in FDTD simulations is considered (41). Instead of the more continuous plasmon excitation profile which is observed in limitless structures considered in analytical models, the following strategy shows us the numerous discrete resonator-like plasmon multipoles. Nevertheless, an LSPR beginning from the round tip summit from the wavelengths in the UV region can be perceived in all cases. Just about recently, Yang et al (41, 42). and Kazemi-Zanjani et al (41, 43) have applied FDTD to explain the localized augmentation of tips in the existence and non-existence of metallic surfaces. Both studies exhibit that field augmentation is concentrated at the summit of the tip when the surface is dielectric, and spatial restriction of the gap plasmon begin to be observable in the existence of a metallic surface.

Meng et al. used FDTD, along with experiments, to show that EM augmentation of up to 10^5 can be obtained using an uncovered AFM tip just to stress on the significance of the selection of materials on the EM in TERS. The phenomenon can be accredited to the lightning rod effect (44). They also proposed what they thought to be the most favorable configuration for Au-coated AFM tip-substrate system. They discovered that a 5 nm layer of Au on a Si AFM tip bring about the best augmentation when they improved the efficiency of the tip, incident field, and substrate. The result balanced tip sharpness, and therefore resolution, with the augmentation (44).

It should be taken into account that accepted TERS electrodynamic models should incorporate both the incident as well as the outgoing fields. Schatz and Ausman (45) revealed that dipole reradiation can be the cause to a far-field spatial in homogeneities in the detector signal. When the incident radiation together with the detector are non-orthogonal, these factors become more noticeable.

Depending on different types of scanning probe microscopy, TERS can be divided into two types. They are briefly described in the following two sections.

2.4.2 AFM-Based TERS

Diffraction limit always hinders us from getting the ultimate resolution of an object through optical microscopy. Over the years after, a vast amount of researches scientists have come out with some legit solutions. Atomic-force microscopy (AFM) or scanning force microscopy (SFM) is one of them. It is a type of scanning probe microscopy (SPM) which measure the resolution in sub-wavelength range, and the result is almost 1000 times better than the diffraction limit. While performing AFM, a metallic tip is used to get the results by touching the surface, and the tip is attached to a cantilever which is prepared by a piezoelectric material. Usually, the apex of the tip is very sharp and the diameter is about 5nm or less. These tips are coated with metal, commonlyby thermal evaporation under high vacuum (13) or electroless plating (14) techniques.

2.4.3 STM-Based TERS

In STM systems, the probe tips are made of solid metal, usually gold and Silver. It also utilizes gold substrate to control the tunneling current and the tip−sample separation. The apex of the tip is typically about 10 nm, the length is several tens of micrometers, and the tip surface is fairly smooth (46). Therefore, a STM tip can be best considered as a long smooth nanocone, which is not the best nanostructure to enhance visible light, because it is too long compared to the wavelength of the excitation light. However, the proximity of gold substrate in STM creates a metallic nanogap between the tip apex and the substrate, and a strongly enhanced hot spot is created within the nanogap (47-49). Thus, a strong enhancement is achieved in STM-based TERS, which is also benefitted from the high spatial resolution associated with the STM technique. The tip plays dual roles by enhancing the light field and by controlling the tunneling current, which in turn controls the tip−sample separation, however, within the range of a few

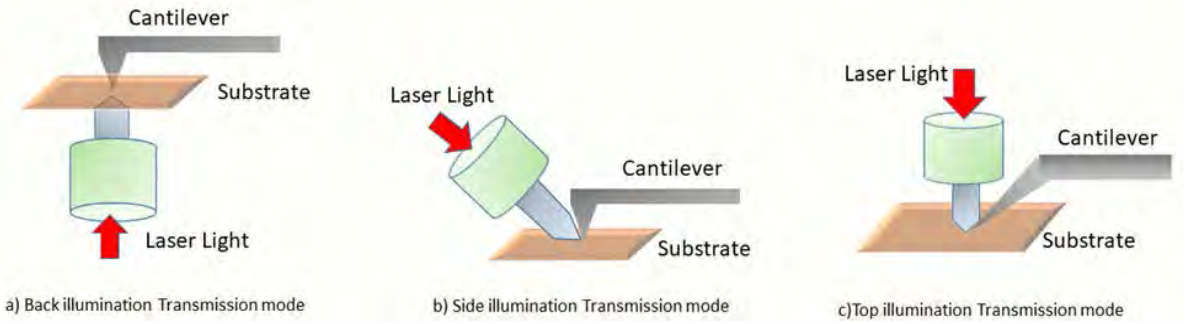

Figure 8: Figure: Different configurations of AFM based TERS (a) source is in the backside (b) illuminating from the side and (C) source is placed on the top.

nanometers. This is not bad for usual TERS measurements, but in some applications, it might be necessary to control the tip− sample separation with larger values. The recent advances of STM techniques also allow high-vacuum and low-temperature measurements, (50) which is advantageous for better stability as well as for observing samples at low temperature. Further, one can easily control the incident polarization to either parallel or perpendicular to the tip axis, if the incident light is at a grazing angle. On the negative side, since the sample is placed on a reasonably thick metallic substrate, which is opaque to the incident light, it is not possible to use the transmission mode with backscattering configuration in STM (46). One therefore needs to utilize the reflection mode with side illumination and side collection configuration. Since this configuration requires a lens with long working distance, it is not possible to use objective lenses with high-NA, and hence it is not possible to tightly focus the incident light on the tip apex. Some groups have used an interesting optical system for STM, where, instead of a lens, they use a parabolic mirror to focus the incident light to the tip apex as well as to collect the Raman signal (50,51). This configuration allows them to slightly improve the size of the focus spot.

2.4.4 Application of TERS in life sciences

Biological Samplers

Even though the biological samples has become more difficult to figure out , TERS analysis of biological compounds has provided us with a very detailed properties of the technique. Furthermore, a lot of elementary properties of TERS originally became clear after studying samples like these (52).

Cells bacteria and viruses

TERS was used in 2006 to analyze biological samples such as epidermal cells . where we could figure out various surface composites regardless of the labels (53).

Primary studies on models which has biological significance for example alginate fibers (bio film) and lipid mixture were thought of as a convenient for the establishment of a database that

allows analysis of these factors in complex biological samples (53, 54-56). The studies also make it clear that even in small volume the weak Raman scatters are being determined by the use of TERS. regarding this, more caution should be taken while measuring bacterial membranes, where there is a danger of tip contamination, so the experiments must be controlled (57). Even while working in dynamic mode miniscule fragments can also be picked up with ease due to this fragile texture .

To get rid of tip contamination , Budich et al proposed that the measurements are controlled on uncovered substrate . The contamination of the tip can be associated with both forming carbonaceous species and collecting sample molecules. these carbon samples also hinder the experiment and must be remove as it will decrease the quality of the sample signals (56).

TERS can also be used to measure same distant points of surface of the cell. it was revealed that using the spectral finger prints from the proteins and lipids we can figure out these molecules and picture how are they distributed. (58). In comparison to far field Raman spectroscopy where bands at 3000 per cm can figure out lipids, TRES is not very effective in that spectral region. In a little wavenumber region (such as 532-488nm for silver and 633-785nm for gold tips) the excited surface plasmons on the TERS tip are most effective when the absorption maximum of the nano particles is equal to the Laser wavelength. SO the bands greater than 2500 per cm doesn't encounter a strong signal amplification. as a result, spectral finger print area is being focused (52). Even with these obstacles being present, Opilik et al. Showed that greater wavenumber areas are accessible and C_H bands could be observed on by lipid layers.

TERS is not strong enough to detect components that are buried, unless its amplified. Molecular Variation on cell membrane couldn't be identified without degrading the sample if wasn't for this specificity of the surface. It was shown by tests on wound healing processed cells that a more detailed image can be found by using organic analysis with near field results (60). Investigation of Inter cellular compartments requires the preparation of cell section. Using this Wood at al. was able to access haemozoin crystals produced from part of cells that r infected by malaria (59). the capability to pinpoint this compound seemed to be very effective for later studies where it requires tracing of anti-malarial drugs that are preferably not detectable to haemozoin.

Protein Based materials

Even excluding the requirement of a gap-mode configuration, the spatial resolution and sensitivity of TERS allows the investigation of an amyloid fibril at sub protein level. STM was used to picture the classification of amino acid. Scanning the surface allowed us to see the presence of phenylalanine that could be projected on nanotubes from beta-amyloid (61, 62) fragments.There are more similarities of TERS spectra of nucleobases that was showed in the Domke's work and SERS than with far field Raman Spectra, whereas Rasmussen's recording of TERS spectra had more similarity with SERS spectra, and neither of the band position shifts and bandwidth broadening.Data taken on samples of nucleobases with higher complexity n homo polymer RNA and DNA single strand and showed that there is a change in spectra when there is movement along the strand (52,63,64). As a consequence of TERS being specific, it was possible to assign various nucleobases on the DNA molecules (52, 64,65) or the deduction of the position between adenine and thymine (52, 66). Moreover, a rough idea of the molecule tip design depending on little change in the spectral of adenine – thymine base pair was enabled because of susceptibility and specificity of TERS.

2.4.5 Advantages of TERS over SERS

In order to detect vibration and chemical information of molecules, the most proficient technique could be availed is 'SERS'. It provides advantageous features over low Raman scattering. However, this technique was further enhanced latter on as it showed few limitations on its processes. Firstly, SERS signals of random adsorbed molecules are the stretched out entities of mean vibrations (67). Particular SERS (SM-SERS), (68, 36) have alteration resulting from different bonds of the molecule entering in and out of the vicinity of hot spot. Many groups are only capable of controlling adsorption of a molecule chemically at a specific locus of nanoparticle. However, it is next to impossible to identify bond of the molecules associated with Raman signal received if theoretical simulations are considered. Adding insult to injury, all of the SM-SERS experiments have been investigated based on statistical analysis. It's really tough to see a particular molecule in an aimed target. Making it difficult to attain absolute resolution of

a molecule in real space (68-70). Furthermore, the samples are vulnerable to get contaminated in air, which might distort analyzed result of identified target molecules. For instance, photo-bleaching or signals from other impurity molecules adsorbed on the samples(71,72).Hence, making it very difficult to distinguish whether a Raman signal is emerged from the target molecules or contaminated from unwanted sources which might give false interpretations.

In order to vanquish the short scope of substrates and spatial resolution in SERS, researchers put their effort to gear up and enhance the scope of SERS. It was first witnessed when Wessel in 1985 first show cased the concept of tip-enhanced Raman scattering (TERS). TERS is the unification of surface enhanced Raman spectroscopy (SERS) and scanning probe microscopy (SPM)(73).

Spatial resolution can be improved using a pointed metal tip while the enhancement factor can still be maintained to identify a distinct molecule. Finally, in 2000 Zenobi, Kawata, Anderson and Pettinger separately presented TERS results. This brought about the feasibility of TERS. (74) TERS dragged further interest from then onwards amongst the researchers around the world. Several groups came across single molecule detection and mapping (75), using Raman signals at single molecular level resolution. But initially the best outcomes were only at the entire molecular resolved level. This was insufficient to identify the particular region of molecules. Subsequently enormous stress was made to extract better resolution, (75, 76) and furthermore TERS was improved into nano-imaging method for surface science, including at the sub-molecular level. There are considerable review papers relating to that. (66, 79).

3. Methodology

There are different types of models are developed in the course of time to solve electromagnetic differential equations. Generally, Maxwell's and Helmholtz's equations are solved in the time domain to discretize the outputs. For this particular thesis, finite difference time domain method was used because it gives a wide range of outputs from a single simulation.

3.1 Finite-Difference-Time-Domain

In this section, the mathematical formulations behind FDTD method is described shortly.

Maxwell's equations are solved in time domain for dielectric materials (27):

$$\frac{\partial \vec{D}}{\partial t} = \nabla \times \vec{H}$$

$$\vec{D}(\omega) = \varepsilon_0 \varepsilon_r(\omega) \vec{E}(\omega)$$

$$\frac{\partial \vec{H}}{\partial t} = -\frac{1}{\mu_0} \nabla \times \vec{E}$$

Here,

$\vec{H}$, represents the magnetic field

$\vec{E}$, represents the electric field and

$\vec{D}$, represents the displacement field

while $\varepsilon_r(\omega)$ is the complex relative dielectric constant ($\varepsilon_r(\omega) = n^2$, where n is the refractive index).

In 3D, Maxwell's equations have six different field components. They are: Ex, Ey, Hz, Hx, Hy, Ez. If we assume that, in the z- direction the dimension is infinite then we can write (27):

$$\varepsilon_r(\omega, x, y, z) = \varepsilon_r(\omega, x, y)$$

$$\frac{\partial \vec{E}}{\partial z} = \frac{\partial \vec{H}}{\partial z} = 0$$

Then Maxwell's equations are divided into transverse electric and transverse magnetics which can be solved in only x-y plane (28):

TE: Ex, Ey, Hz

TM: Hx, Hy, Ez

After reducing the Maxwell's equations, the TM equations look like (29) :

$$\frac{\partial D_z}{\partial t} = \frac{\partial H_y}{\partial x} - \frac{\partial y}{\partial x}$$

$$D_z(\omega) = \varepsilon_0 \varepsilon_r(\omega) E_z(\omega)$$

$$\frac{\partial H_x}{\partial t} = -\frac{1}{\mu_0}\frac{\partial E_z}{\partial y}$$

$$\frac{\partial H_y}{\partial t} = \frac{1}{\mu_0}\frac{\partial E_z}{\partial x}$$

In FDTD method, different field components are solved in a discrete way in different position of Yee cell like the figure above. The electric field components are placed in the edges and magnetic field components are placed in the walls of Yee cell (29).

For this thesis, a tip of 80 nm was used. The radius of the tip was 10 nm and the cone angle was 25^0. The substrate's dimension was 350 nm× 350nm× 10 nm. Ag CRC and Au CRC materials were used in terms as tip and substrate. Two mesh was used, they were named as: 'mesh gap' and 'mesh'. Where, mesh gap was used in between the tip and substrate. On the other hand, 'mesh' was used to cover all the other area. The size of the mesh gap was d_x= 1nm, d_y = 1nm, d_z = 0.4 nm. The calculation of the electric fields was done by summing all the magnitudes from all three directions. Normalized electric field, $|E|^2 = |E_x|^2 + |E_y|^2 + |E_z|^2$ (31).

3.2 Brief description of Lumerical

Introduction

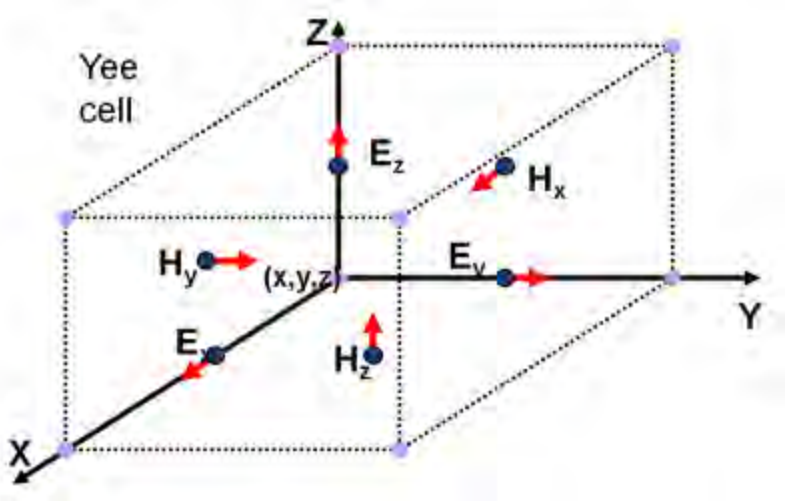

Figure 9: Yee cell (27)

The objective of the thesis was to investigate a tip and then tip and substrate simultaneously for mapping the Tip-enhanced Raman spectroscopy and observing the effect of the polarization of the sources.

After installing and opening the FDTD solutions software, four windows opened each introducing its own perspective. The upper left window indicates XY view while the upper right window indicates the 3D view of the particle. The lower left window indicates the XZ view and lower right window indicates the YZ view.

Simulation region

The background index was kept default to 1. Simulation time was kept 25fs and the dimension was 3D. The dimension of the simulation region was set to 400nm × 400 nm× 268 nm. In the mesh settings, mesh accuracy was set to 2 because the higher order of the mesh accuracy requires more memory and time. After that, in order to lowering the memory and time the boundary condition was manipulated. Boundary condition at the minimum of the x axis was set to Anti-symmetric but in the maximum side it was set to perfectly matched layer. In the boundary of minimum y, the condition was symmetric but at the maximum boundary it was set to perfectly matched layer. At the minimum of z axis, the condition was metal and the maximumof z, the boundary condition was set to perfectly matched layer.

Mesh

FDTD Solutions in Lumerical uses a rectangular, Cartesian style mesh to calculate the fundamental quantities like electric and magnetic fields at its each points. The smaller the size of the mesh, the higher the required memory. In this thesis, two meshes were used to simulate. They are ‘Mesh gap’ and ‘Mesh’ by name. The dimension of override meshes the ‘Mesh gap’ was 1nm × 1 nm × 0.4nm and ‘Mesh’ was 5nm in override mesh dimension.

Objects

For the sake of simulation two materials were used from the Lumerical library. They are Silver (Ag CRC) and Gold (Au CRC).

Source

Total field scattered field source was used as the illuminating source. The reason behind using this is, it can distinguish the scattered field from the total field which makes the whole task lot easier.

Monitors

To preserve the simulation data and observe the enhancements, different 2D monitors were appointed. One was normal to the Y-axis and another normal to the X-axis. Dimension of the monitors were same. Depending on different simulations, their wavelengths were changed time to time.

4. Results

4.1 Impact of polarization in FDTD simulations

The polarization of the source beam plays an important role in the electric field in the vicinity of the tip. The intensity and distribution depend on it. Linearly and radially polarized sources in different TERS configurations have been considered to examine the effect.

4.1.1 Radial Polarization

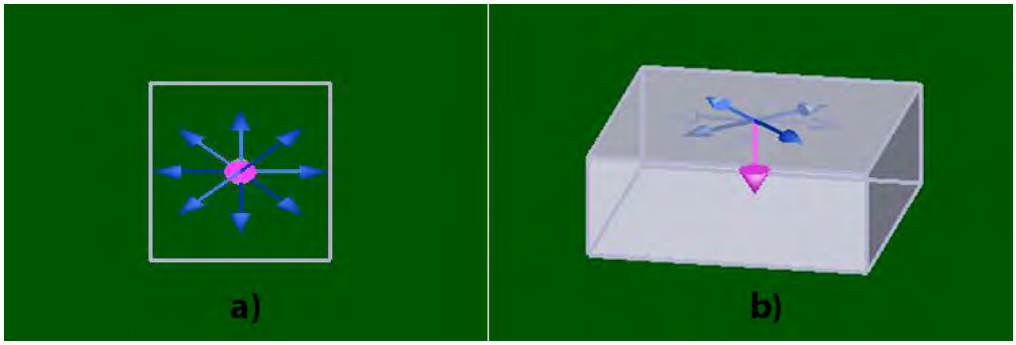

Figure 10: a) Top view of the radially polarized source, b) Perspective view of the source. White encompassed region denotes the simulation region.

In a radially polarized source, the polarization vectors are oriented radially in the transverse plane with respect to the propagation direction.

The white encompassed area reperesents a focused radially polarized source inside the FDTD simulation region. Many concentric rings with different intensities and lowest intensity at the middle form the transverse component of theradially polarized source. On the other hand, the longitudinal component also consists of rings with fewer intensities than the transverse components. The enhancement comes from the interaction between the longitudinal component and the apex of the tip. In FDTD package of Lumerical there is no radially polarized source. That is why, four linearly polarized TFSF sources were integrated to make a single radially polarized source.

4.1.2 Linear Polarization

Electric field vectors in the linearly polarized source are oriented along only one direction of

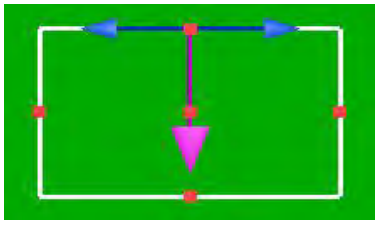

Figure 11: Linearly Polarized Total Field Scattered Field light source. White boundary represents the simulation area

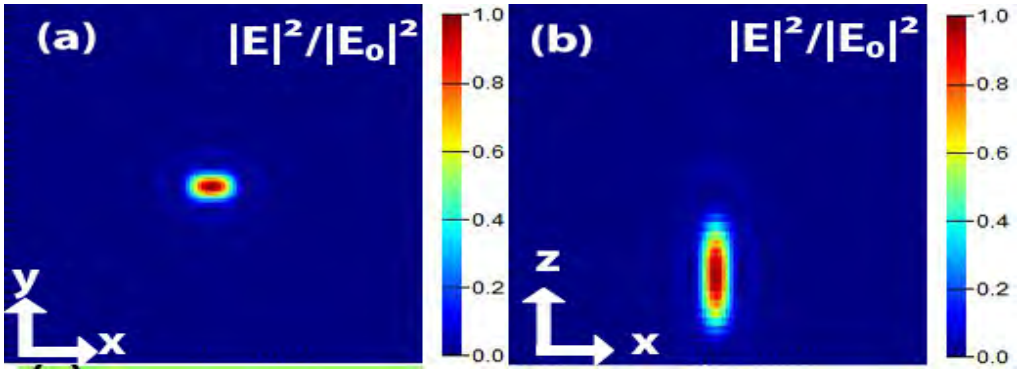

Figure 12: Electric field density of normalized total field polarized in x-direction (a) top view (b) side view.

propagation.

The figure above shows the top view and side view of a Gaussian source which is consisted of several concentric ring having the highest intensity in the middle.

4.2 Normalization of Electric Field Intensity

Every electric intensity in the next section are normalized. For simulations where a plane wave has been utilized, the intensity of the source is by default equal to 1 as a presumption in FDTD program. Therefore, for all the simulations performed by a linearly polarized light, the FDTD output for intensities is already normalized to the intensity of the source. In case of radially polarized sources however, the intensity of the source should be determined in accordance with the FDTD output after the source is created. After the source intensity $|E_0|^2$, is determined, the estimated electric field magnitude for each simulation, $|E\ |^2$, was normalized to the source

intensity through $|E\ \ |^2/|E_0|^2$.

4.3 FDTD Calculations of Electric field

As we know that there is an important effect of polarization on the enhancement of electric field and overall TERS measurements. For investigating that effect, linearly and radially polarized beams were used in this experiment. After doing all the experiments the electric field enhancements were compared that are found from linearly and radially polarized sources to come to a conclusion.

4.3.1 Effect of linear polarization on enhancement factor on tip only

A total field scattered field source was used to examine the effect of linear polarization. It was placed perpendicular to the tip, the direction of propagation was along the vertical line of the tip.

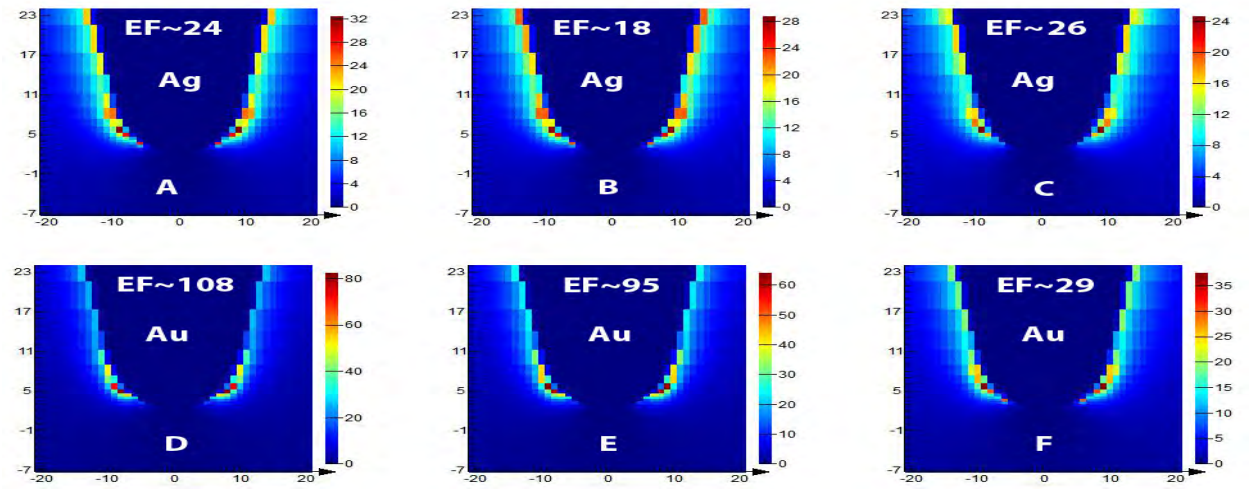

Figure 13: Electric field distribution at the apex of the tip. Tip radius is 10nm, height is 80nm and linearly polarized light source along the tip axis (A) Ag tip with normalized enhancement factor 24 at 532 nm wavelength (B) Ag tip with normalized enhancement factor 18 at 550 nm wavelength (c) Ag tip with normalized enhancement factor 26 at 632 nm wavelength (D) Au tip with normalized enhancement factor 108 at 532 nm wavelength (E) Au tip with normalized enhancement factor 95 at 550 nm wavelength and (F) Au tip with normalized enhancement factor 29 at 632 nm wavelength.

The source was placed along the z-axis and the direction was backward. The amplitude of the source was normalized (amplitude was set to 1). The simulation area of the source was set to 350 nm×350 nm×220nm. After running the simulation the following results have been found.

In the figure we can see that, due to linear polarization of the source there is no enhancement in the middle of the tip rather electric field in the two sides of the tip are enhanced. This phenomena happens for both silver (Ag) and gold (Au) tip.

4.3.2 Effect of radial polarization on enhancement factor on tip only

Four total field scattered field sources were integrated to form a radially polarized source. For this, the transverse components of all the sources were oriented 35^{o} apart from each other. This

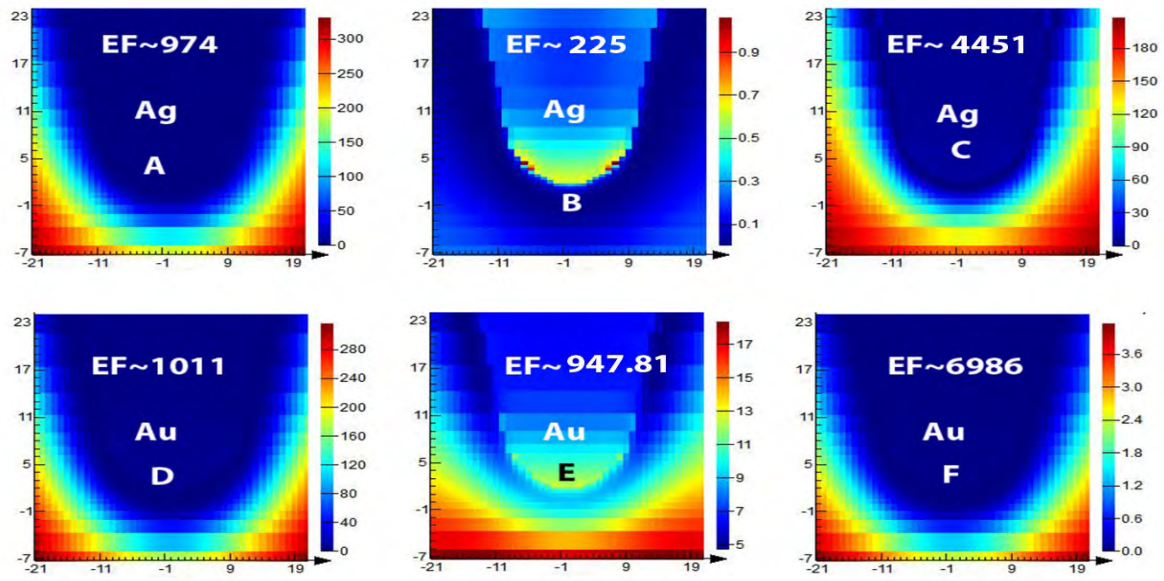

Figure 14: Electric field distribution at the apex of the tip. Tip radius is 10nm, height is 80nm and radially polarized light source along the tip axis (A) Ag tip with normalized enhancement factor 974 at 532 nm wavelength (B) Ag tip with normalized enhancement factor 225 at 550 nm wavelength (c) Ag tip with normalized enhancement factor 4451 at 632 nm wavelength (D) Au tip with normalized enhancement factor 1011 at 532 nm wavelength (E) Au tip with normalized enhancement factor 947.81 at 550 nm wavelength and (F) Au tip with normalized enhancement factor 6989 at 632 nm wavelength.

source was then used to examine the effect of radial polarization. It was placed perpendicular to the tip, the direction of propagation was along the vertical line of the tip. The source was placed

along the z-axis and the direction was backward. The amplitude of the source was normalized (amplitude was set to 1). The simulation area of the source was 350 nm×350 nm×220nm. After completing the simulation, the following images have been found.

In the above figure, when the source is polarized radially the enhancement occurs at the middle of the tip. Though, the significant amount of enhancement occurred in the image (F) the confinement is very low here. On the other hand, in figure (B) the confinement is better.

4.3.3 Effect of linear polarization on enhancement factor in the Gap mode:

In this mode, all the aspects of the source and tip were kept same. In addition to that, a substrate was introduced which has a dimension of 400 nm×400 nm× 10 nm. The following results were found after running the simulation.

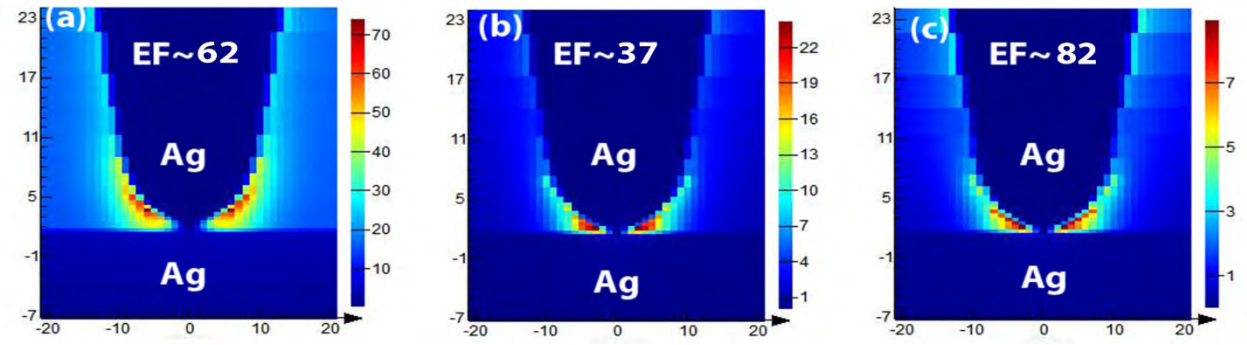

Figure 15: Electric field distribution at the apex of the tip in the gap mode. The distance between the tip and substrate is about 1nm. Tip radius is 10nm, height is 80nm and linearly polarized light source along the tip axis (a) Ag tip with normalized enhancement factor 62 at 532 nm wavelength (b) Ag tip with normalized enhancement factor 37 at 550 nm wavelength (c) Ag tip with normalized enhancement factor 82 at 632 nm wavelength

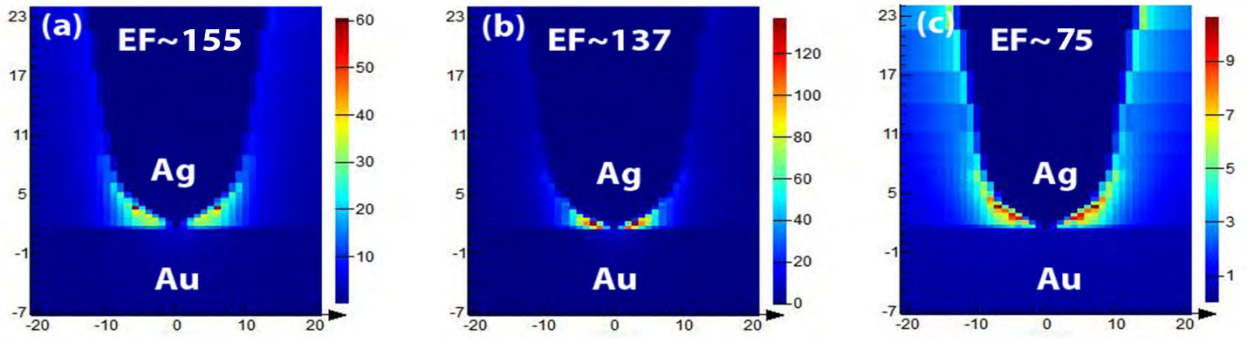

Figure 16: Electric field distribution at the apex of the tip in the gap mode. The distance between the tip and substrate is about 1nm. Tip radius is 10nm, height is 80nm and linearly polarized light source along the tip axis (a) Ag tip with normalized enhancement factor 155 at 532 nm wavelength (b) Ag tip with normalized enhancement factor 137 at 550 nm wavelength (c) Ag tip with normalized enhancement factor 75 at 632 nm wavelength

From the above images it is obvious that Ag-Ag combination has the highest enhancement factor

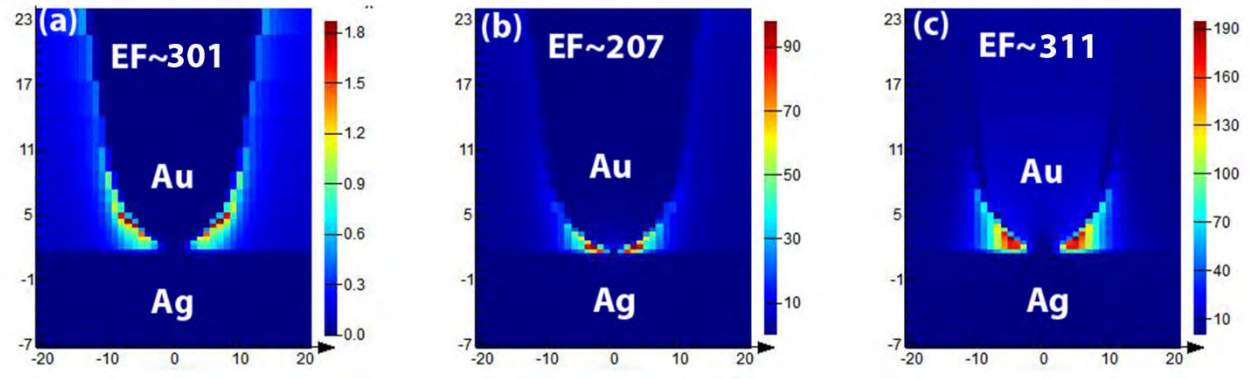

Figure 17: Electric field distribution at the apex of the tip in the gap mode. The distance between the tip and substrate is about 1nm. Tip radius is 10nm, height is 80nm and linearly polarized light source along the tip axis (a) Au tip with normalized enhancement factor 301 at 532 nm wavelength (b) Au tip with normalized enhancement factor 207 at 550 nm wavelength (c) Au tip with normalized enhancement factor 311 at 632 nm wavelength.

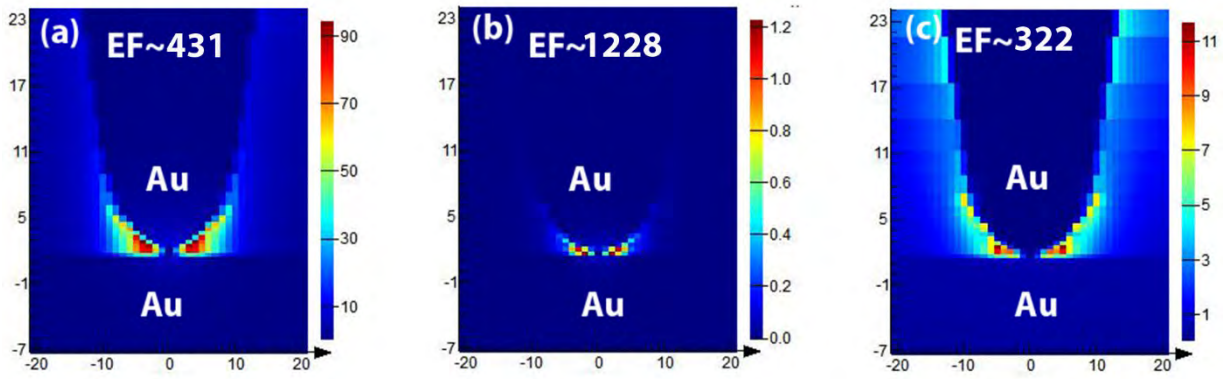

Figure 18: Electric field distribution at the apex of the tip in the gap mode. The distance between the tip and substrate is about 1nm. Tip radius is 10nm, height is 80nm and linearly polarized light source along the tip axis (a) Au tip with normalized enhancement factor 431 at 532 nm wavelength (b) Au tip with normalized enhancement factor 1228 at 550 nm wavelength (c) Ag tip with normalized enhancement factor 322 at 632 nm wavelength

at 532 nm wavelength, for Ag-Au the highest enhancement factor is 137 at 550 nm wavelength and the highest enhancement factor is 156, at 550 nm wavelength Au-Au has the highest enhancement factor and lastly Au-Ag has the enhancement factor of 431 at 532 nm wave length which is the highest.

4.3.4 Effect of radial polarization on enhancement factor in the Gap Mode

The same radially polarized source and tip-substrate were in this section. After running the simulation for about 15 minutes for each, the following figures have been found.

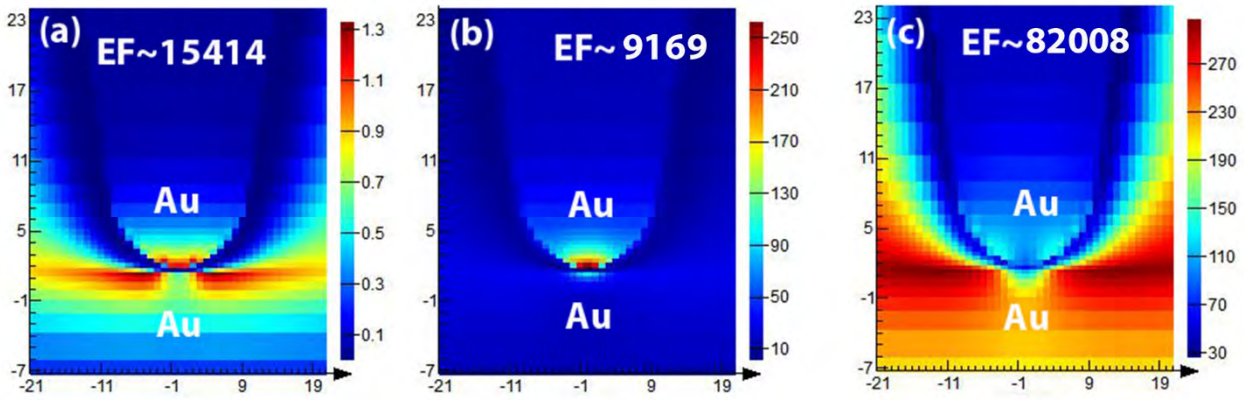

Figure 20: Electric field distribution at the apex of the tip in the gap mode. The distance between the tip and substrate is about 1nm. Tip radius is 10nm, height is 80nm and radially polarized light source along the tip axis (a) Au tip with normalized enhancement factor 15414 at 532 nm wavelength (b) Au tip with normalized enhancement factor 9169 at 550 nm wavelength (c) Au tip with normalized enhancement factor 82008 at 632 nm wavelength.

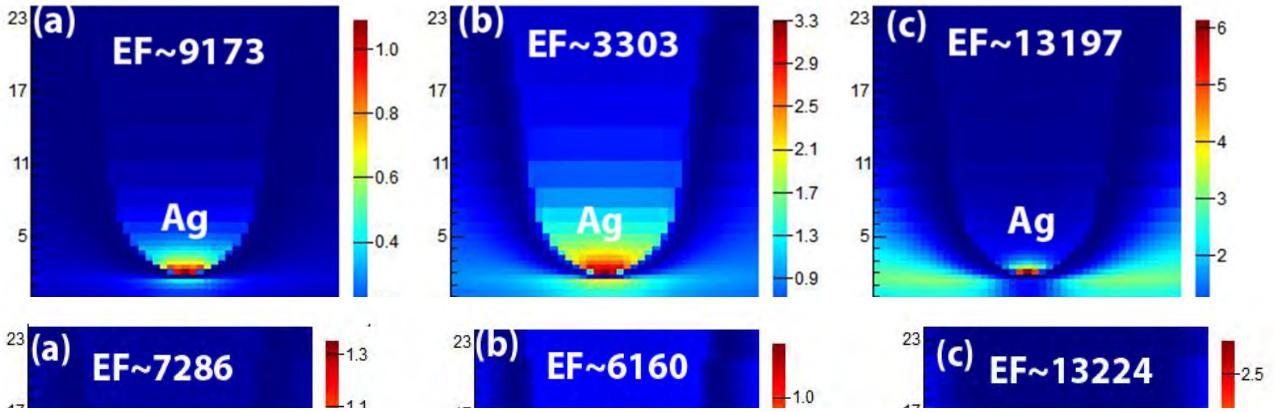

Figure 21: Electric field distribution at the apex of the tip in the gap mode. The distance between the tip and substrate is about 1nm. Tip radius is 10nm, height is 80nm and radially polarized light source along the tip axis (a) Ag tip with normalized enhancement factor 9173 at 532 nm wavelength (b) Ag tip with normalized enhancement factor 3303 at 550 nm wavelength (c) Au tip with normalized enhancement factor 13197 at 632 nm wavelength.

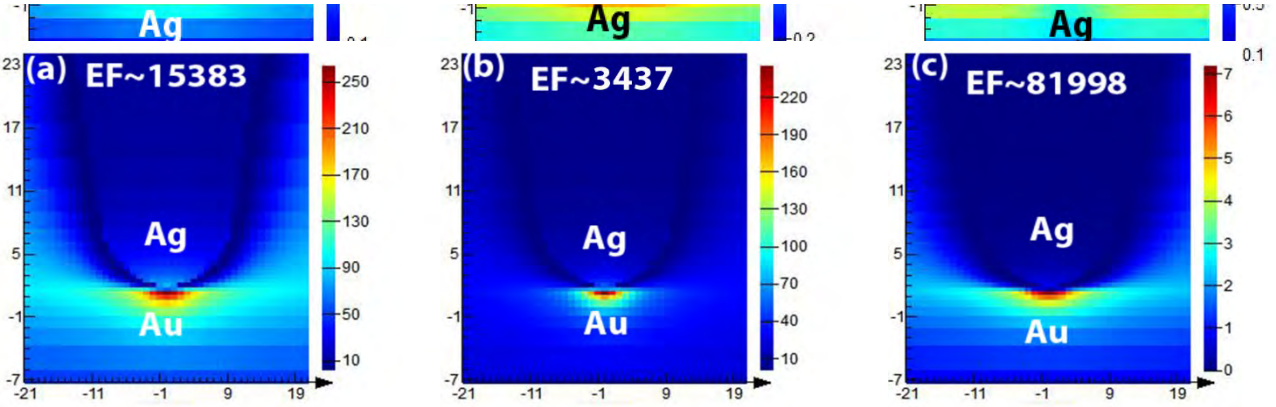

Figure 22: Electric field distribution at the apex of the tip in the gap mode. The distance between the tip and substrate is about 1nm. Tip radius is 10nm, height is 80nm and radially polarized light source along the tip axis (a) Ag tip with normalized enhancement factor 15383 at 532 nm wavelength (b) Au tip with normalized enhancement factor 3437 at 550 nm wavelength (c) Au tip with normalized enhancement factor 81998 at 632 nm wavelength.

From the above images it is obvious that Au-Ag combination has the highest enhancement at632.8 nm wavelength, for Au-Au the highest enhancement is 82008 at 550 nm wavelength and the highest enhancement is 13197, at 550 nm wavelength Au-Au has the highest enhancement and lastly Au-Ag has the enhancement factor of 81998 at 532 nm wave length which is the highest.

4. Discussion

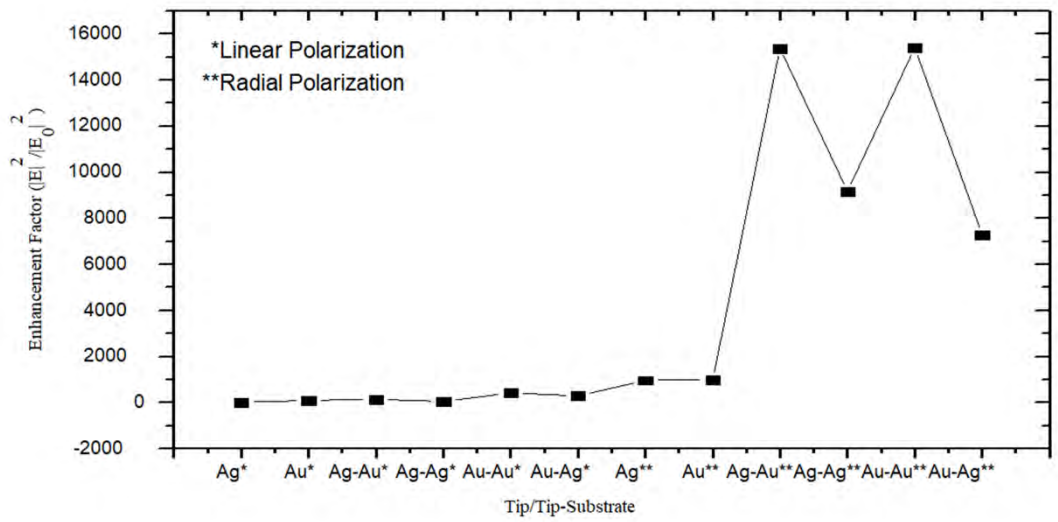

Figure 23: All the enhancement factors at 532 nm wavelength.

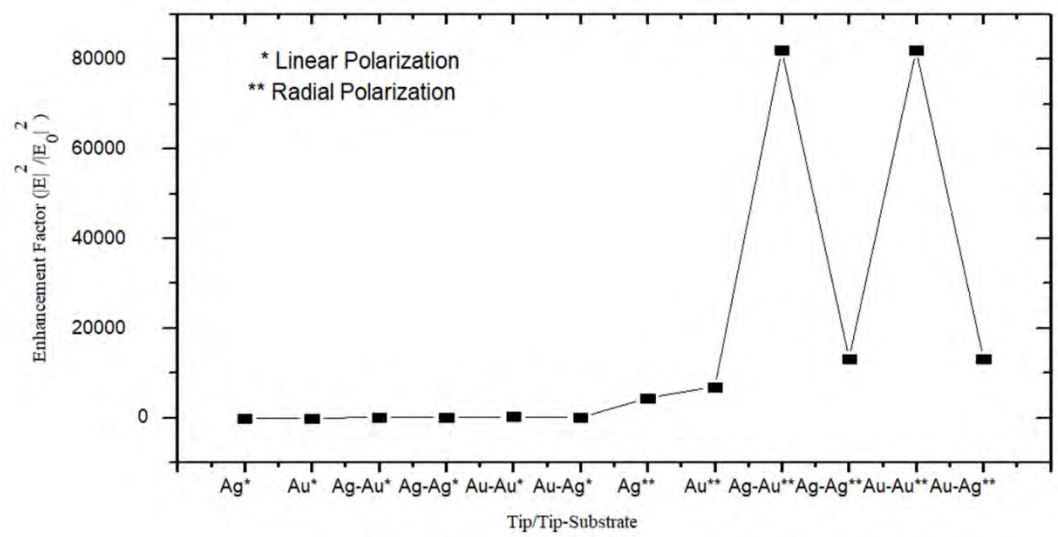

In the previousall the results were shown in details. In this section with the help of graphical representation, the results were discussed thoroughly.

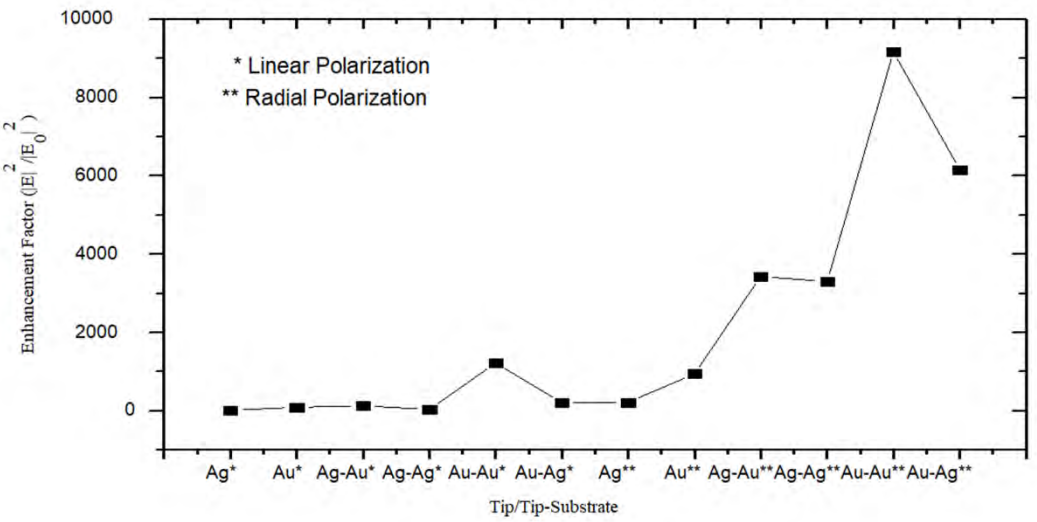

Figure 25: All the enhancement factors at 632 nm wavelength.

By a close inspection, it can be observed two common things in all of the illustrations above. They are, radial polarization increases enhancement factor than linear polarization in a significantly large amount. In addition to that, whenever Gold (Au) is used as substrate it enhances signal more than a Silver (Ag) substrate.

The result can be justified by the use of absorption coefficient. Absorption coefficient can be written as

(78),

Figure 24: All the enhancement factors at 550 nm wavelength.

$$Absorption \quad \frac{4\pi n}{k\lambda} \text{ …….. (4) (78)}$$

Where, n is the refractive index, λ is wavelength and k is the extinction coefficient.

For, 532 nm, 550 nm and 632 nm wavelength the absorption coefficient of Ag and Au is calculated with the help of the data from (78) and presented in tables below:

Table 1: Absorption Coefficient of Silver (Ag)

Wavelength	Refractive index (n)	Extinction coefficient(k)	Absorption coefficient (α)
532 nm	0.129	3.25	0.595
550 nm	0.126	3.45	0.626
632 nm	0.140	4.15	0.589

Table 2: Absorption Coefficient of Gold (Au)

Wavelength	Refractive index (n)	Extinction coefficient(k)	Absorption coefficient (α)
532 nm	0.402	2.54	0.149
550 nm	0.306	2.88	0.215
632 nm	0.166	3.15	0.377

From the tables we can see that, at 532 nm wavelength Ag has an absorption constant of 0. 595.Whereas, at the same wavelength Au has an absorption constant of only 0.149. The same trend goes on for 550 nm and 632 nm wavelength. As a result, when, Au as substrate it is absorbing less and scattering more light than Au. That is why, every time Au gives more enhancement than Ag

This page was intentionally left blank

4. Conclusion

Through the simulation localized electric field in the vicinity of the metallic tip of TERS was examined and the effect of different polarization of source in mapping TERS was observed. From the observation, it can be concluded that, radial polarization is more effective for enhancing the local electric field because it gives better enhancement as well as better confinement which is ideal for tip-enhanced Raman spectroscopy. Another observation is, Ag and Au both plays an important role in increasing the enhancement factor but Au gives more enhancement due to its low absorption constant.

References

[1] Chen, X., Liu, Y., Huang, J., Liu, W., Huang, J., Zhang, Y. and Fu, W. (2017). Label-free techniques for laboratory medicine applications. Frontiers in Laboratory Medicine, 1(2), pp.82-85.

[2] Horiba.com. (2017). Raman Application Notes and Articles - HORIBA. [online] Available at: http://www.horiba.com/scientific/products/raman-spectroscopy/applications/ [Accessed 18 Nov. 2017].

[3] Acharya, S., Maheshwari, N., Tatikondewar, L., Kshirsagar, A. and Kulkarni, S. (2013). Ethylenediamine-Mediated Wurtzite Phase Formation in ZnS. Crystal Growth & Design, 13(4), pp.1369-1376.

[4] Wood, B., Langford, S., Cooke, B., Lim, J., Glenister, F., Duriska, M., Unthank, J. and McNaughton, D. (2004). Resonance Raman Spectroscopy Reveals New Insight into the Electronic Structure ofβ-Hematin and Malaria Pigment. Journal of the American Chemical Society, 126(30), pp.9233-9239.

[5] Kitt, J., Bryce, D., Minteer, S. and Harris, J. (2017). Raman Spectroscopy Reveals Selective Interactions of Cytochrome c with Cardiolipin That Correlate with Membrane Permeability. Journal of the American Chemical Society, 139(10), pp.3851-3860.

[6] Casiraghi, C., Piazza, F., Ferrari, A., Grambole, D. and Robertson, J. (2005). Bonding in hydrogenated diamond-like carbon by Raman spectroscopy. Diamond and Related Materials, 14(3-7), pp.1098-1102.

[7] Stellarnet.us. (2017). Available at: https://www.stellarnet.us/wp-content/uploads/Exp4_Raman.pdf [Accessed 18 Nov. 2017].

[8] D. P. Woodruff and T. A. Delchar, Modern Techniques of Surface Science, Cambridge

University Press, 1994.

[9] Z. Zhang, S. Sheng, R. Wang and M. Sun, "Tip-Enhanced Raman Spectroscopy", Analytical Chemistry, vol. 88, no. 19, pp. 9328-9346, 2016.

[10] Kudelski, A.; Pettinger, B. Chem. Phys. Lett. 2000, 321, 356−362.

[11] Etchegoin, P. G.; Lacharmoise, P. D.; Le Ru, E. C. Anal. Chem.

2009, 81, 682−688.

[12] Detection Of Drugs Of Abuse In Saliva By Surface-enhanced ... (n.d.). Retrieved from http://journals.sagepub.com/doi/abs/10.1366/11-06310 Itzkan, I.; Dasari, R.; Feld, M. S. Phys. Rev. Lett. 1997, 78, 1667−1670.

[13] Pubsdc3.acs.org. (n.d.). Retrieved from HTTP://pubsdc3.acs.org/doi/full/10.1021/acs.analchem.6b02093?src=recsys2194−2198

[14] Lim, D. K.; Jeon, K. S.; Kim, H. M.; Nam, J. M.; Suh, Y. D. Nat. Mater. 2010, 9, 60−67.

The non-destructive and in-situ analysis of pigments. Berlin: Horiba, 2017, pp. 1-4.

[15] Osa | Tip-enhanced Photoluminescence Spectroscopy Of ... (n.d.). Retrieved from https://www.osapublishing.org/prj/abstract.cfm?URI=prj-5-6-745Raman Spectroscopy", Analytical Chemistry, vol. 88, no. 19, pp. 9328-9346, 2016.

[16] R. Stöckle, Y. Suh, V. Deckert and R. Zenobi, "Nanoscale chemical analysis by tip-enhanced Ramanspectroscopy," Chemical Physics Letters, vol. 318, no. 1-3, pp. 131-136, 2000.

[17] Vance, M. (2017). Raman Spectroscopy of Nanotechnology. [online] Virginia Tech Sustainable Nanotechnology. Available at: http://blogs.lt.vt.edu/sustainablenano/2014/08/19/raman-spectroscopy-in-nanotechnology/ [Accessed 4 Nov. 2017].

[18] A. Zrimsek, N. Chiang, M. Mattei, S. Zaleski, M. McAnally, C. Chapman, A. Henry, G. Schatz and R. Van Duyne, "Single-Molecule Chemistry with Surface- and Tip-Enhanced Raman Spectroscopy," Chemical Reviews, vol. 117, no. 11, pp. 7583-7613, 2016.

[19] Vandenabeele, P. (2013). Practical Raman Spectroscopy. Hoboken: Wiley, p.32.

[20] Schuster, K., Reese, I., Urlaub, E., Gapes, J. and Lendl, B. (2000). Multidimensional Information on the Chemical Composition of Single Bacterial Cells by Confocal Raman Microspectroscopy. Analytical Chemistry, 72(22), pp.5529-5534.

[21] Caspers, P., Lucassen, G. and Puppels, G. (2003). Combined In Vivo Confocal Raman Spectroscopy and Confocal Microscopy of Human Skin. Biophysical Journal, 85(1), pp.572-580.

[22] Butler, H., Ashton, L., Bird, B., Cinque, G., Curtis, K., Dorney, J., Esmonde-White, K., Fullwood, N., Gardner, B., Martin-Hirsch, P., Walsh, M., McAinsh, M., Stone, N. and Martin, F. (2016). Using Raman spectroscopy to characterize biological materials. Nature Protocols, 11(4), pp.664-687.

[23] Čukovska, L., Minčeva - Šukarova, B., Lluveras-Tenorio, A., Andreotti, A., Colombini, M. and Nastova, I. (2012). Micro-Raman and GC/MS analysis to characterize the wall painting technique of Dicho Zograph in churches from the Republic of Macedonia. Journal of Raman Spectroscopy, 43(11), pp.1685-1693.

[24] Ding, J., Xu, T., Tan, X., Jin, H., Shao, J. and Li, H. (2017). Raman spectrum: A potential biomarker for embryo assessment during in vitro fertilization. Experimental and Therapeutic Medicine, 13(5), pp.1789-1792.

[25] Raman Spectroscopy to Aid In Selecting Viable Sperm For Ivf. (n.d.). Retrieved from https://www.medgadget.com/2009/01/raman_spectroscopy_to_aid_in_selecting_viable_

[26] Bhavya Sharma, Renee R. Frontiera, Anne-Isabelle Henry, Emilie Ringe, Richard P. Van Duyne, SERS: Materials, applications, and the future, In Materials Today, Volume 15, Issues 1–2, 2012, Pages 16-25, ISSN 1369-7021, https://doi.org/10.1016/S1369-7021(12)70017-(http://www.sciencedirect.com/science/article/pii/S1369702112700172)

[27] Kb.lumerical.com. (2017). FDTD | Lumerical Knowledge Base. [online] Available at: https://kb.lumerical.com/en/solvers_finite_difference_time_domain.html [Accessed 22 Dec. 2017].

[28] Sullivan, D. M. (2013). *Electromagnetic Simulation Using the FDTD Method*. Hoboken, NJ: Wiley-Blackwell.

[29] Taflove, A. (1995). Computational electrodynamics. Boston: Artech House.

[30] Gedney, S. (2013). Introduction to the Finite-difference Time-domain (Fdtd) Method for Electromagnetics. EBSCOhost.

[31] KazemiZanjani, Nastaran, "Tip-Enhances Raman Spectroscopy, Enabling Spectroscopy at the Nanoscale" (2014). *Electronic Thesis and Dissertation Repository*. 2079.

[32] Novotny, L. and Hecht, B. (n.d.). *Principles of nano-optics*.

[33] Mayer, K. and Hafner, J. (2011). Localized Surface Plasmon Resonance Sensors. Chemical

Reviews, 111(6), pp.3828-3857.

[34] Zrimsek, A., Henry, A. and Van Duyne, R. (2013). Single Molecule Surface-Enhanced Raman Spectroscopy without Nanogaps. *The Journal of Physical Chemistry Letters*, 4(19), pp.3206-3210.

[35] Chemistry World. (2017). *Sers and the rise of the Raman empire*. [online] Available at: https://www.chemistryworld.com/feature/sers-and-the-rise-of-the-raman-empire/9264.article [Accessed 22 Dec. 2017].

[36] Stiles, P., Dieringer, J., Shah, N. and Van Duyne, R. (2008). Surface-Enhanced Raman Spectroscopy. *Annual Review of Analytical Chemistry*, 1(1), pp.601-626.

[37] Encyclopedia Britannica. (2017). *Luminescence - Luminescence physics | physics*. [online] Available at: https://www.britannica.com/science/luminescence/Luminescence-physics [Accessed 22 Dec. 2017].

[38] Haynes, C., McFarland, A. and Duyne, R. (2005). Surface-Enhanced Raman Spectroscopy. *Analytical Chemistry*, 77(17), pp.338 A-346 A.

[39] Campion, A. and Kambhampati, P. (1998). Surface-enhanced Raman scattering. *Chemical Society Reviews*, 27(4), p.241.

[40] Sharma, B., Frontiera, R., Henry, A., Ringe, E. and Van Duyne, R. (2012). SERS: Materials, applications, and the future. *Materials Today*, 15(1-2), pp.16-25.

[41] Pozzi, E., Goubert, G., Chiang, N., Jiang, N., Chapman, C., McAnally, M., Henry, A., Seideman, T., Schatz, G., Hersam, M. and Duyne, R. (2016). Ultrahigh-Vacuum Tip-Enhanced Raman Spectroscopy. *Chemical Reviews*, 117(7), pp.4961-4982.

[42] Yang, Z., Aizpurua, J. and Xu, H. (2009). Electromagnetic field enhancement in TERS configurations. *Journal of Raman Spectroscopy*, 40(10), pp.1343-1348.

[43] Kazemi-Zanjani, N., Vedraine, S. and Lagugné-Labarthet, F. (2013). Localized enhancement of electric field in tip-enhanced Raman spectroscopy using radially and linearly polarized light. *Optics Express*, 21(21), p.25271.

[44] Meng, L., Huang, T., Wang, X., Chen, S., Yang, Z. and Ren, B. (2015). Gold-coated AFM tips for tip-enhanced Raman spectroscopy: theoretical calculation and experimental demonstration. *Optics Express*, 23(11), p.13804.

[45] Ausman, L. and Schatz, G. (2009). On the importance of incorporating dipole reradiation in the modeling of surface enhanced Raman scattering from spheres. *The Journal of Chemical Physics*, 131(8), p.084708.

[46] Verma, P. (2017). Tip-Enhanced Raman Spectroscopy: Technique and Recent

Advances. *Chemical Reviews*, 117(9), pp.6447-6466.

[47] Michaels, A., Jiang and Brus, L. (2000). Ag Nanocrystal Junctions as the Site for Surface-Enhanced Raman Scattering of Single Rhodamine 6G Molecules. *The Journal of Physical Chemistry B*, 104(50), pp.11965-11971.

[48] Xu, H., Bjerneld, E., Käll, M. and Börjesson, L. (1999). Spectroscopy of Single Hemoglobin Molecules by Surface Enhanced Raman Scattering. *Physical Review Letters*, 83(21), pp.4357-4360.

[49] Xu, H., Aizpurua, J., Käll, M. and Apell, P. (2000). Electromagnetic contributions to single-molecule sensitivity in surface-enhanced Raman scattering. *Physical Review E*, 62(3), pp.4318-4324.

[50] Klingsporn, J., Jiang, N., Pozzi, E., Sonntag, M., Chulhai, D., Seideman, T., Jensen, L., Hersam, M. and Duyne, R. (2014). Intramolecular Insight into Adsorbate–Substrate Interactions via Low-Temperature, Ultrahigh-Vacuum Tip-Enhanced Raman Spectroscopy. *Journal of the American Chemical Society*, 136(10), pp.3881-3887.

[51] Zhang, D., Wang, X., Braun, K., Egelhaaf, H., Fleischer, M., Hennemann, L., Hintz, H., Stanciu, C., Brabec, C., Kern, D. and Meixner, A. (2009). Parabolic mirror-assisted tip-enhanced spectroscopic imaging for non-transparent materials. *Journal of Raman Spectroscopy*, 40(10), pp.1371-1376.

[52] Deckert-Gaudig, T., Taguchi, A., Kawata, S. and Deckert, V. (2017). Tip-enhanced Raman spectroscopy – from early developments to recent advances. *Chemical Society Reviews*, 46(13), pp.4077-4110.

[53] Neugebauer, U., Rösch, P., Schmitt, M., Popp, J., Julien, C., Rasmussen, A., Budich, C. and Deckert, V. (2006). On the Way to Nanometer-Sized Information of the Bacterial Surface by Tip-Enhanced Raman Spectroscopy. *ChemPhysChem*, 7(7), pp.1428-1430.

[54] Schmid, T., Burkhard, J., Yeo, B., Zhang, W. and Zenobi, R. (2008). Towards chemical analysis of nanostructures in biofilms I: imaging of biological nanostructures. *Analytical and Bioanalytical Chemistry*, 391(5), pp.1899-1905.

[55] Schmid, T., Messmer, A., Yeo, B., Zhang, W. and Zenobi, R. (2008). Towards chemical analysis of nanostructures in biofilms II: tip-enhanced Raman spectroscopy of alginates. *Analytical and Bioanalytical Chemistry*, 391(5), pp.1907-1916.

[56] Opilik, L., Bauer, T., Schmid, T., Stadler, J. and Zenobi, R. (2011). Nanoscale chemical imaging of segregated lipid domains using tip-enhanced Raman spectroscopy. *Physical Chemistry Chemical Physics*, 13(21), p.9978.

[57] BUDICH, C., NEUGEBAUER, U., POPP, J. and DECKERT, V. (2008). Cell wall investigations utilizing tip-enhanced Raman scattering. *Journal of Microscopy*, 229(3), pp.533-

539.

[58] Richter, M., Hedegaard, M., Deckert-Gaudig, T., Lampen, P. and Deckert, V. (2010). Laterally Resolved and Direct Spectroscopic Evidence of Nanometer-Sized Lipid and Protein Domains on a Single Cell. *Small*, 7(2), pp.209-214.

[59] Wood, B., Bailo, E., Khiavi, M., Tilley, L., Deed, S., Deckert-Gaudig, T., McNaughton, D. and Deckert, V. (2011). Tip-Enhanced Raman Scattering (TERS) from Hemozoin Crystals within a Sectioned Erythrocyte. *Nano Letters*, 11(5), pp.1868-1873.

[60] Watkins-Mariani, M., Deckert-Gaudig, T. and Deckert, V. (2014). Label-free in vitro visualization and characterization of caveolar bulbs during stimulated re-epithelialization. *Analytical and Bioanalytical Chemistry*, 406(27), pp.6993-7002.

[61] Albrecht, M. and Creighton, J. (1977). Anomalously intense Raman spectra of pyridine at a silver electrode. *Journal of the American Chemical Society*, 99(15), pp.5215-5217.

[62] Sonntag, M., Klingsporn, J., Zrimsek, A., Sharma, B., Ruvuna, L. and Van Duyne, R. (2014). Molecular plasmonics for nanoscale spectroscopy. *Chem. Soc. Rev.*, 43(4), pp.1230-1247.

[63] Bailo, E. and Deckert, V. (2008). Tip-Enhanced Raman Spectroscopy of Single RNA Strands: Towards a Novel Direct-Sequencing Method. *AngewandteChemie International Edition*, 47(9), pp.1658-1661.

[64] Treffer, R., Lin, X., Bailo, E., Deckert-Gaudig, T. and Deckert, V. (2011). Distinction of nucleobases – a tip-enhanced Raman approach. *Beilstein Journal of Nanotechnology*, 2, pp.628-637.

[65] Hennemann, L., Meixner, A. and Zhang, D. (2010). Surface- and tip-enhanced Raman spectroscopy of DNA. *Spectroscopy*, 24(1-2), pp.119-124.

[66] Zhang, D., Domke, K. and Pettinger, B. (2010). Tip-Enhanced Raman Spectroscopic Studies of the Hydrogen Bonding between Adenine and Thymine Adsorbed on Au (111). *ChemPhysChem*, 11(8), pp.1662-1665.

[67] Zhang, Z., Sheng, S., Wang, R. and Sun, M. (2016). Tip-Enhanced Raman Spectroscopy. *Analytical Chemistry*, 88(19), pp.9328-9346.

[68] Kneipp, K., Wang, Y., Kneipp, H., Perelman, L., Itzkan, I., Dasari, R. and Feld, M. (1997). Single Molecule Detection Using Surface-Enhanced Raman Scattering (SERS). *Physical Review Letters*, 78(9), pp.1667-1670.

[69] Zrimsek, A., Henry, A. and Van Duyne, R. (2013). Single Molecule Surface-Enhanced Raman Spectroscopy without Nanogaps. *The Journal of Physical Chemistry Letters*, 4(19), pp.3206-3210.

[70] Lim, D., Jeon, K., Kim, H., Nam, J. and Suh, Y. (2009). Nanogap-engineerable Raman-active nanodumbbells for single-molecule detection. *Nature Materials*, 9(1), pp.60-67.

[71] Kudelski, A. and Pettinger, B. (2000). SERS on carbon chain segments: monitoring locally surface chemistry. *Chemical Physics Letters*, 321(5-6), pp.356-362.

[72] Etchegoin, P., Lacharmoise, P. and Le Ru, E. (2009). Influence of Photostability on Single-Molecule Surface Enhanced Raman Scattering Enhancement Factors. *Analytical Chemistry*, 81(2), pp.682-688.

[73] Wessel, J. (1985). Surface-enhanced optical microscopy. *Journal of the Optical Society of America B*, 2(9), p.1538.

[74] Stöckle, R., Suh, Y., Deckert, V. and Zenobi, R. (2000). Nanoscale chemical analysis by tip-enhanced Raman spectroscopy. *Chemical Physics Letters*, 318(1-3), pp.131-136.

[75] Pozzi, E., Sonntag, M., Jiang, N., Klingsporn, J., Hersam, M. and Van Duyne, R. (2013). Tip-Enhanced Raman Imaging: An Emergent Tool for Probing Biology at the Nanoscale. *ACS Nano*, 7(2), pp.885-888.

[76] Fang, Y., Zhang, Z. and Sun, M. (2016). High vacuum tip-enhanced Raman spectroscope based on a scanning tunneling microscope. *Review of Scientific Instruments*, 87(3), p.033104.

[77] Deckert-Gaudig, T. and Deckert, V. (2016). High resolution spectroscopy reveals fibrillation inhibition pathways of insulin. *Scientific Reports*, 6(1).

[78] Ecse.rpi.edu. (2017). [online] Available at: https://www.ecse.rpi.edu/~schubert/Educational-resources/Materials-Refractive-index-and-extinction-coefficient.pdf [Accessed 22 Dec. 2017].